Propagation of structural uncertainty to linear aeroelastic stability

3 AUTHORS, INCLUDING:

Hamed Haddad Khodaparast
Swansea University

42 PUBLICATIONS   **215** CITATIONS

SEE PROFILE

John Mottershead
University of Liverpool

244 PUBLICATIONS   **4,555** CITATIONS

SEE PROFILE

Propagation of structural uncertainty to linear aeroelastic stability

Hamed Haddad Khodaparast *, John E. Mottershead, Kenneth J. Badcock

Department of Engineering, University of Liverpool, Harrison-Hughes Building, The Quadrangle, Liverpool L69 3GH, United Kingdom

ARTICLE INFO

ABSTRACT

The problem of linear flutter analysis in the presence of structural uncertainty is addressed. Whereas the propagation of uncertain structural parameters in finite element models has been carried out by a number of different methods, there appears to be less published work on the influence of random structural parameters on flutter speed. In this paper, we first evaluate the sensitivity of aeroelastic damping to a number of uncertain structural, geometrical and structural-damping parameters. The most significant parameters are identified and then randomised. Secondly, interval, fuzzy and probabilistic methods are used to propagate the structural uncertainty through the aeroelastic analysis resulting in regions of flutter-boundary uncertainty characterised by intervals, fuzzy membership functions and probability density functions. Interval analysis requires two optimisation procedures in order to find the bounds of the aeroelastic responses. The *Response Surface Method* (RSM) permits efficient optimisation and is used for the estimation of the gradient and Hessian. The resulting intervals are checked using *Monte–Carlo Simulation* (MCS). Probabilistic analysis is carried out using both first- and second-order perturbation, using the gradient and the Hessian determined by RSM. The first-order perturbation method is generally found to produce results in good agreement with the MCS, although there are differences at the tails of the distributions, especially for the unstable modes close to the flutter speed. The second-order perturbation method provides an improved prediction of the nonlinear behaviour at the tails. The flutter membership function predicted by the fuzzy method generally includes the nonlinear behaviour at the tails of the MCS distribution. Variability in structural mass and stiffness parameters is shown to have a significant effect upon the flutter intervals. Structural damping results in a small but significant increase in the flutter speed, but structural-damping variability does not translate into significant intervals of flutter-boundary uncertainty. Studies are carried out on the Goland wing, with and without structural damping, and on a generic fighter model.

1. Introduction

The accurate estimation of flutter boundaries is an important problem in aircraft certification. When the structural model includes parameter uncertainties, represented by intervals, fuzzy membership functions or probability density functions, then this uncertainty may be propagated through the aeroelastic model resulting in uncertain flutter boundaries, described correspondingly in terms of intervals, fuzzy memberships and probability densities. The review paper by Pettit [1] and references therein show the considerable attention that has already been paid to this subject. This paper is specifically concerned with aeroelastic analysis in the presence of structural uncertainty, and the evaluation of various propagation methods.

There are generally two classes of uncertainty, epistemic and aleatoric (irreducible) uncertainty [2]. The main cause of epistemic uncertainty is lack of knowledge, reducible by further information.

Lack of confidence arising from either the choice of computational aeroelastic method or the fidelity of modelling assumptions is a form of epistemic uncertainty. Variability in structural parameters arising from the accumulation of manufacturing tolerances or environmental erosion is aleatoric. Structural variability must be characterised and the first step in achieving this is to discover which of the uncertain structural parameters have a significant affect on the aeroelastic analysis. The distribution or range of these parameters must be estimated. This variability may then be propagated through the model to determine a distribution or range of flutter speeds. In a small number of research papers [1] flutter-speed estimates are determined in the presence of parameter uncertainty. Poirion [3] used a first-order perturbation method to calculate the probability of flutter for given uncertainty in structural properties. The estimated flutter probability density function obtained by the perturbation method was found not to be in good agreement with MCS results. Kurdi et al. [4] used MCS to propagate the variation in dimensional properties of the structural parameters of the Goland wing in order to quantify the flutter-speed probability density function. Results showed the flutter speed to be

---

* Corresponding author.
*E-mail address:* H.Haddad-Khodaparast@liverpool.ac.uk (H.H. Khodaparast).

Table 1
Nominal values of thicknesses and areas for the Goland wing finite element model.

Parameter	Thickness ft (m)	Parameter	Area ft^2 (m^2)
Upper and lower wing skins	0.0155 (0.0047)	Leading and trailing edge spar caps	0.0416 (0.003865)
Leading and trailing edge spars	0.0006 (0.00018)	Centre spar cap	0.1496 (0.013898)
Centre spar	0.0889 (0.0271)	Rib caps	0.0422 (0.003921)
Ribs	0.0347 (0.01058)	Posts	0.0008 (0.000074)

Table 2
Flutter speed bounds from different methods.

Mach	Lower bound of flutter speed ft/s ($\times 0.3\,048$ m/s)					Mean flutter Speed ft/s ($\times 0.3048$ m/s)					Upper bound of flutter speed ft/s ($\times 0.3048$ m/s)				
	MCS	Pb 1st	Pb 2nd n	Pb 2nd p	Fuzzy	MCS	Pb 1st	Pb 2nd n	Pb 2nd p	Fuzzy	MCS	Pb 1st	Pb 2nd n	Pb 2nd p	Fuzzy
0.7	387.0	393.5	392.8	390.9	374.0	417.1	417.1	416.5	416.5	417.1	443.4	440.8	440.2	440.6	463.0
0.8	365.5	366.0	366.3	366.5	349.3	388.7	387.4	387.8	387.8	387.4	415.2	408.9	409.2	411.9	430.9
0.825	357.8	357.7	356.6	354.1	340.1	379.2	379.0	378.0	378.0	379.0	401.6	400.2	399.3	400.2	419.8
0.85	346.3	347.1	347.4	346.2	331.1	368.2	366.9	367.2	367.2	366.9	390.7	386.7	387.0	388.0	407.4
0.88	334.7	333.5	333.7	332.3	319.3	353.8	352.7	353.0	353.0	352.7	375.0	372.0	372.3	373.4	390.6
0.90	321.3	326.0	325.4	323.9	312.1	343.6	343.4	342.9	342.9	343.4	363.5	360.9	360.3	360.7	378.6
0.92	318.2	317.9	317.5	316.2	306.1	335.1	334.6	334.3	334.3	334.6	355.4	351.4	351.1	351.6	366.9
0.94	314.8	314.4	314.2	314.2	304.1	330.1	329.1	329.1	329.1	329.1	346.2	343.8	343.9	345.6	358.0
0.95	315.5	314.8	314.8	314.2	306.0	329.7	328.7	328.7	328.7	328.7	344.8	342.6	342.7	343.8	355.5
0.96	316.2	316.0	315.9	315.9	307.7	330.5	329.6	329.6	329.6	329.6	344.6	343.1	343.2	343.6	354.9
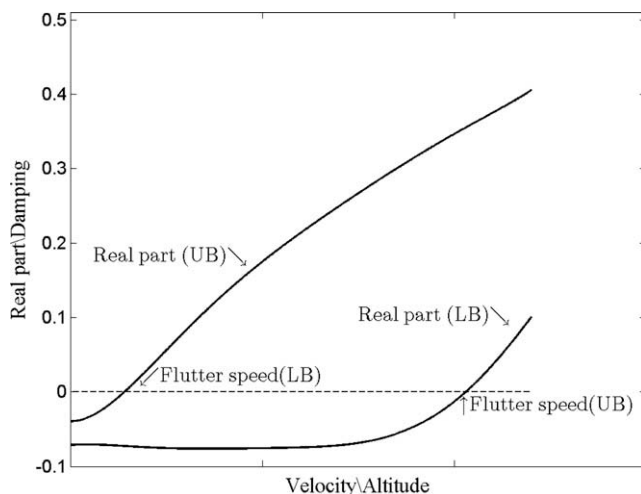
Fig. 1. Flutter speeds bounds and real parts of the flutter mode bounds.

highly sensitive to small changes in the structure. Attar and Dowell [5] used a response surface method to identify the effect of uncertainty on the response of a nonlinear aeroelastic system. Results were found to be in good agreement with those obtained by MCS. Wang et al. [6] considered the problem of flutter analysis in the presence of structural uncertainty using a CFD-based aerodynamic reduced-order model. They evaluated probability density functions for the flutter speeds of the Goland wing by randomizing the stiffness matrix. More recently, Verhoosel et al. [7] used stochastic finite element models to perform uncertainty and reliability analysis on fluid-structure stability boundaries. They found the sensitivity-based methods capable of characterising the statistical moments of the aeroelastic response.

In this paper a sensitivity study is carried out to select those uncertain structural parameters that influence the aeroelastic response considerably. Then three different approaches are considered for the characterisation of flutter-speed uncertainty. In the first approach, an interval flutter analysis is used. This method is said to be 'possibilistic' since no assumption is made about the probability distribution of either the structural parameters or the

flutter speeds. Consequently the interval flutter method is restricted to the evaluation of upper and lower bounds without providing any information on how the uncertainty is distributed within such bounds. The interval flutter analysis requires a minimisation and a maximization of the aeroelastic response. The second approach makes use of fuzzy logic so that the uncertainty is defined according to a membership function. The fuzzy finite element method, introduced by Chen and Rao [8], has been used recently by Moens and Vandepitte [9] for the calculation of uncertain frequency response functions of damped structures. The fuzzy method is implemented within a number of α-levels for the numerical solution of the underlying interval finite element problem. Efficient optimisation procedures make use of the *Response Surface Method* (RSM) [10], which generally produces more accurate estimates of the gradient and Hessian than numerical estimation by finite differences. The third procedure is a probabilistic perturbation approach that makes use of the theory of quadratic forms [11,12]. Each solution of the flutter equation is perturbed about the mean values of the uncertain parameters through a truncated Taylor series expansion. Then the statistical moments of the aeroelastic responses are calculated. The procedure requires the calculation of the gradient and Hessian, which is estimated using RSM. When the perturbation is limited to the first-order terms of the Taylor series there is no need to calculate the Hessian matrix.

In the present article the three propagation methods are applied to the Goland wing [4] and to a model of a fighter aircraft. It is found in these examples that variability in structural damping has less effect on flutter speed intervals than does variability in structural mass and stiffness. Results achieved by first-order perturbation are found to be in good agreement with those obtained from MCS for the eigenvalues of those modes that do not contribute to the flutter. However there are differences at the tails of the distributions for the flutter modes, close to the flutter speed. The nonlinearity at the tails of the probability density functions can be estimated by both second-order perturbation and fuzzy methods. The study in reference [4] used MCS for propagation of structural uncertainty. This method is computationally expensive and may not be feasible for aeroelastic analysis using CFD. In this paper it is shown that the combination of interval analysis and RSM can be considered as a reliable and efficient tool for propagation of
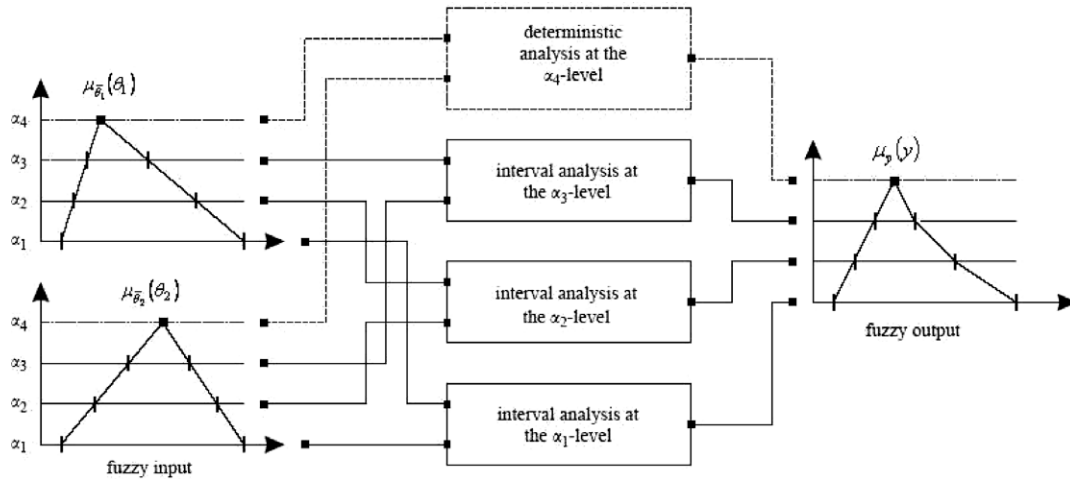
Fig. 2. α-Level strategy, with 4 α-levels, for a function of two triangular fuzzy parameters [9].
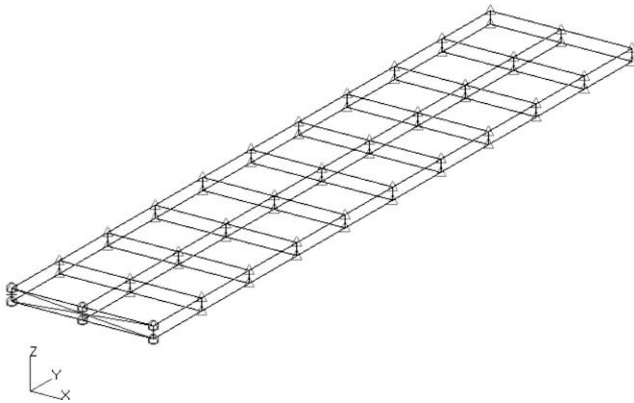

Fig. 3. Finite element model of Goland wing.

structural uncertainty to aeroelastic analysis. The forward propagation methods described here may be used for non-linear aeroelasticity when CFD is used for the aerodynamics, to be reported in a subsequent paper.

2. Flutter and sensitivity analysis using the response surface method (RSM)

Flutter analysis was carried out using the aerodynamic module of MSC-NASTRAN, exploiting the double-lattice subsonic lifting surface theory (DLM), described by Albano and Rodden [13]. The standard linear aeroelastic equation for modal flutter analysis by the PK-method, available in the aeroelastic module of MSC-NAS-TRAN [14], may be expressed as follows,

$$\left[\mathbf{M}\lambda^2 + \left(-\frac{1}{4}\rho\bar{c}V\mathbf{B}/k + \mathbf{C}\right)\lambda + \left(-\frac{1}{2}\rho V^2\mathbf{E} + \mathbf{K}\right)\right](\mathbf{u}) = \mathbf{0} \quad (1)$$
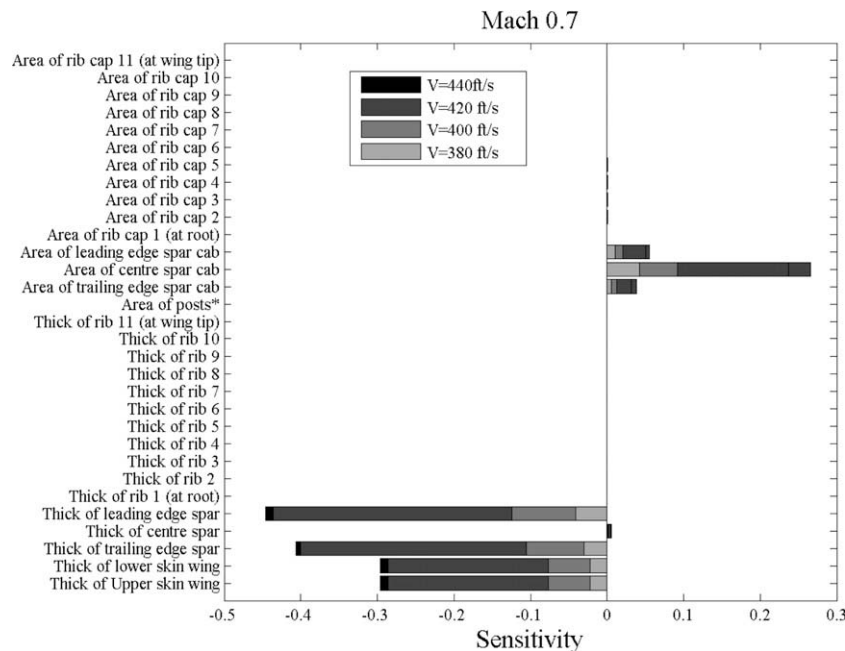

Fig. 4. Aeroelastic damping sensitivity at different velocities (mode 1) – [*]only the greatest sensitivity among 33 posts is shown.
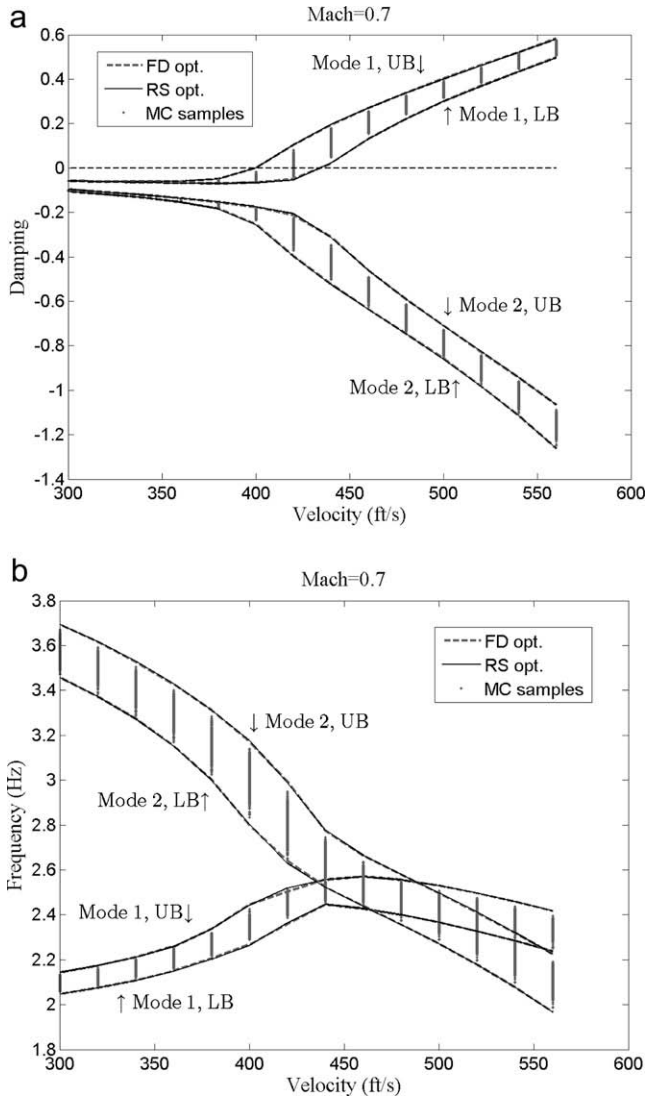
Fig. 5. Interval and MCS results for (a) damping and (b) circular frequency for modes 1 and 2.

Fig. 6. Interval and MCS results showing flutter speeds versus Mach values.

where **M**, **B**, **E**, **C** and **K** are respectively the modal mass, modal aerodynamic damping, modal aerodynamic stiffness, modal structural damping and modal structural stiffness matrices. **B** and **E** are functions of the Mach number and reduced velocity. A complete list of symbols is given in Appendix A. Eq. (1) may be cast in state-space form as,

$$[\mathbf{A}(\omega) - \lambda \mathbf{I}](\mathbf{u}) = \mathbf{0} \tag{2}$$

where,

$$\mathbf{A} = \begin{bmatrix} \mathbf{0} & \mathbf{I} \\ -\mathbf{M}^{-1}\left[-\frac{1}{2}\rho V^2 \mathbf{E} + \mathbf{K}\right] & -\mathbf{M}^{-1}\left[-\frac{1}{4}\rho \bar{c} V \mathbf{B}/k + \mathbf{C}\right] \end{bmatrix} \tag{3}$$

Eq. (2) describes a nonlinear eigenvalue problem. The reduced frequency k is a function of circular frequency, $k = \bar{c}\omega/2V$. The eigenvalue λ may be expressed as $\lambda = \omega(\gamma \pm i)$ where ω is circular frequency and γ is transient decay rate coefficient, or damping. The purpose of this paper is to investigate the flutter analysis of the stochastic system, when **M**, **C** and **K** in Eq. (1) are random matrices. The solution of the complex stochastic eigenvalue problem [15] usually relies upon the availability of the gradient (or sensitivity) and the Hessian. Sensitivity analysis may be used to select those uncertain structural parameters that are most significant. The
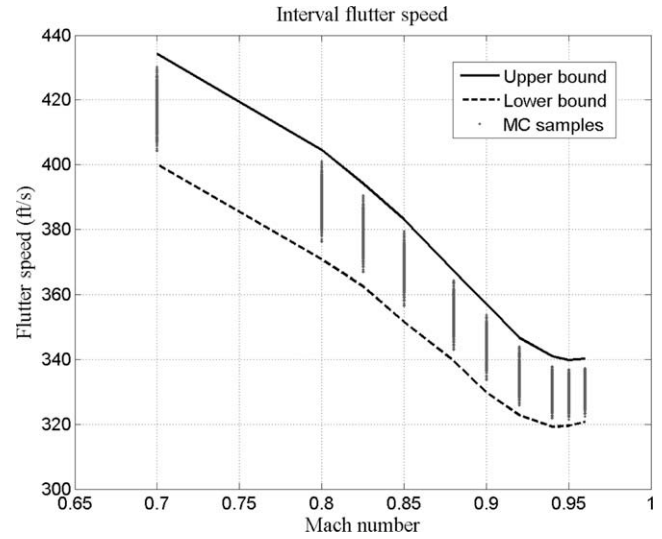
flutter sensitivity, the rate of change of damping γ with respect to changes in the structural parameters θ_j, may be computed by using MSC-NASTRAN. Eq. (1) is then differentiated with respect to parameters and the quantity $\partial\gamma/\partial\theta_j$ determined. The solution is semi-analytical with derivatives approximated using forward differences [14]. The rate of change of the circular frequency ω and flutter speed with respect to changes in the structural parameters θ_j and the second-order sensitivities, not available in MSC-NASTRAN, may be calculated using forward finite differences or alternatively, and usually more accurately, by RSM as will now be described.

Since this paper is concerned with the problem of flutter analysis under the influence of structural variability, the RSM [10] may be used to approximate the aeroelastic responses such as eigenvalues or flutter speeds versus uncertain structural parameters within the region of their variation. In general, the aeroelastic response variable y(eigenvalues or flutter speeds) may be defined as the summation of functions of uncertain structural parameters with regression coefficients β_i as,

$$y(\boldsymbol{\theta}) = \sum_{i=0}^{n} \beta_i f_i(\boldsymbol{\theta}) + \varepsilon \tag{4}$$

where $\boldsymbol{\theta} \in \mathfrak{R}^{m \times 1}$ is the vector of uncertain structural parameters. The method of least squares may be used to estimate the regression coefficients in Eq. (4). For small uncertainties in structural parameters some low-order polynomial form may be chosen for the functions in Eq. (4). For example, the quadratic response surface may be used for the aeroelastic model with m paramers as:

$$y(\boldsymbol{\theta}) = \beta_0 + \sum_{i=1}^{m} \beta_i \theta_i + \sum_{i=1}^{m} \beta_{ii} \theta_i^2 + \sum_{i<j} \sum_{j=2}^{m} \beta_{ij} \theta_i \theta_j + \varepsilon$$
$$= \beta_0 + \mathbf{b}^T \boldsymbol{\theta} + \boldsymbol{\theta}^T \mathbf{B} \boldsymbol{\theta} + \varepsilon \tag{5}$$

where,

$$\mathbf{b} = [\beta_1 \ \beta_2 \ldots \beta_m]^T$$

$$\mathbf{B} = \begin{bmatrix} \beta_{11} & \frac{\beta_{12}}{2} & \cdots & \frac{\beta_{1m}}{2} \\ & \beta_{22} & \cdots & \frac{\beta_{2m}}{2} \\ & & \ddots & \vdots \\ sym. & & & \beta_{mm} \end{bmatrix}$$

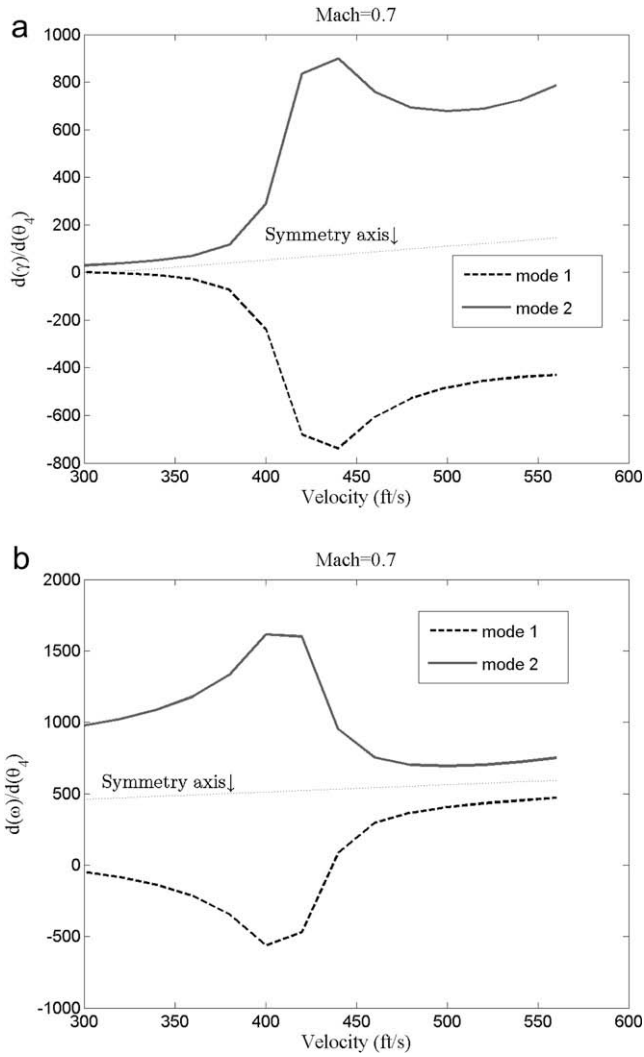$$\underline{\boldsymbol{\theta}} \leqslant \boldsymbol{\theta} \leqslant \bar{\boldsymbol{\theta}}$$

Fig. 7. The sensitivities of (a) damping and (b) circular frequency for modes 1 and 2 with respect to thickness of leading spar edge.
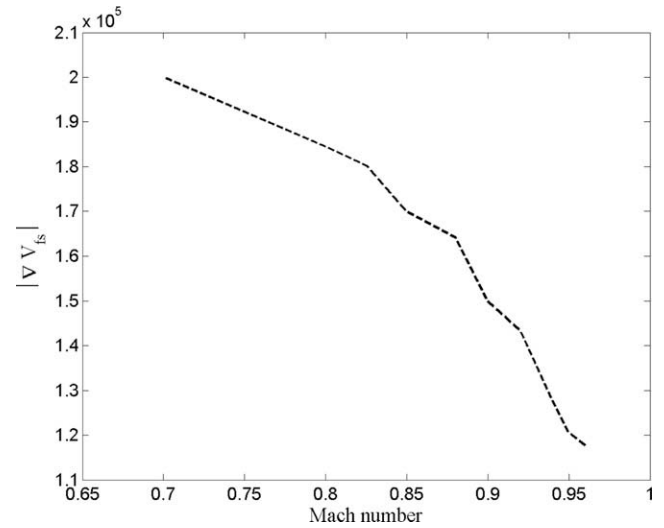

Fig. 8. The norm of sensitivity vector of flutter speed with respect to uncertain parameters at different Mach numbers.
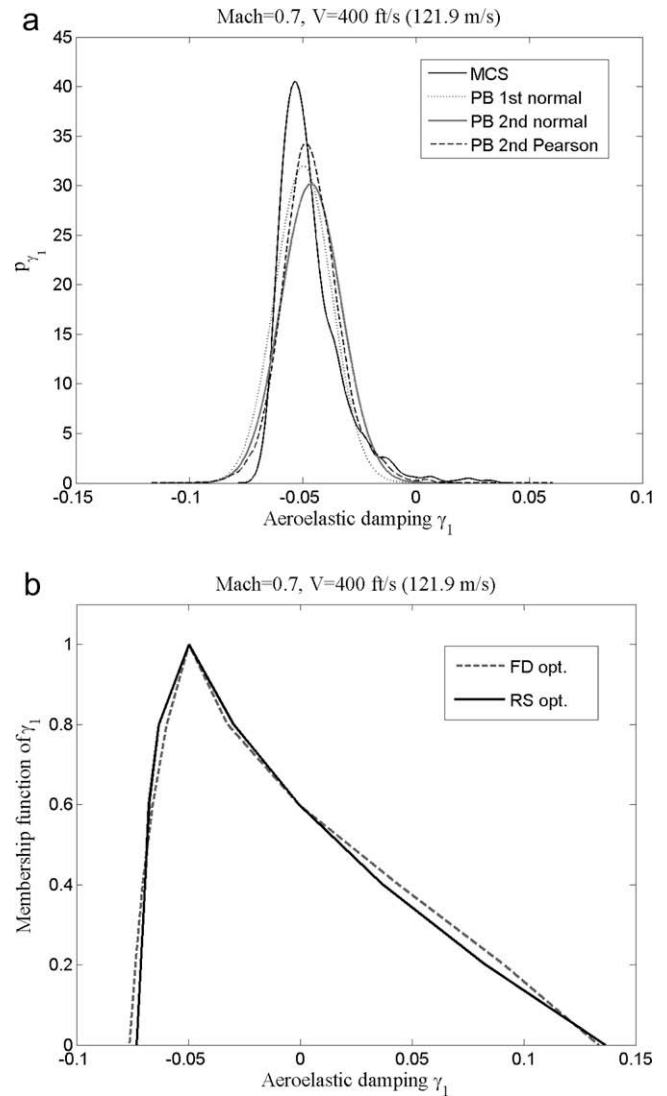
Fig. 9. Aeroelastic damping at velocity 400 ft/s (121.9 m/s): (a) pdfs obtained by 1st and 2nd order perturbation and MCS (b) membership function obtained by RSM and FD optimisation.

where $\underline{\bullet}$ and $\overline{\bullet}$ represent the lower and upper bounds of $\bullet$. The quadratic model includes $(m + 1)(m + 2)/2$ regression coefficients. Therefore the number of samples n, taken from the space of structural parameters, should be greater than $(m + 1)(m + 2)/2$ for an over-determined least-squares solution. The aeroelastic response data may be obtained by solving the deterministic flutter equation for samples selected from the space of uncertain structural parameters. Therefore Eq. (5) can be rearranged to provide a system of overdetermined linear equations as,

$$\mathbf{y} = \mathbf{\Theta}\boldsymbol{\beta} + \boldsymbol{\varepsilon} \tag{6}$$

where,

$$\mathbf{\Theta} = \begin{bmatrix} 1 & \theta_{11} & \theta_{12} & \ldots & \theta_{1m} & \theta_{11}^2 & \theta_{12}^2 & \ldots & \theta_{1m}^2 & \theta_{11} \times \theta_{12} & \ldots & \theta_{1(m-1)} \times \theta_{1m} \\ 1 & \theta_{21} & \theta_{22} & \ldots & \theta_{2m} & \theta_{21}^2 & \theta_{22}^2 & \ldots & \theta_{2m}^2 & \theta_{21} \times \theta_{12} & \ldots & \theta_{2(m-1)} \times \theta_{2m} \\ \vdots & \vdots & \vdots & & \vdots & \vdots & \vdots & & \vdots & \vdots & & \vdots \\ 1 & \theta_{n1} & \theta_{n2} & \ldots & \theta_{nm} & \theta_{n1}^2 & \theta_{n2}^2 & \ldots & \theta_{nm}^2 & \theta_{n1} \times \theta_{n2} & \ldots & \theta_{n(m-1)} \times \theta_{nm} \end{bmatrix}$$

$$\mathbf{y} = [y_1 \, y_2 \ldots y_n]^T$$

and n represents the number of samples. Minimising the vector of residuals ε with respect to coefficients $\boldsymbol{\beta}$ leads to:

$$\boldsymbol{\beta} = (\mathbf{\Theta}^T\mathbf{\Theta})^{-1}\mathbf{\Theta}^T\mathbf{y} \tag{7}$$

The sensitivity vector, $\mathbf{g}(\boldsymbol{\theta}) = \left\{\frac{\partial y}{\partial \theta_j}\right\}$, and the Hessian matrix, $\mathbf{G}(\boldsymbol{\theta}) = \left[\frac{\partial^2 y}{\partial \theta_j \partial \theta_k}\right]$, may now be estimated by differentiating Eq. (5) with respect to structural parameters,

$$\mathbf{g}(\boldsymbol{\theta}) = \mathbf{b} + 2\mathbf{B}\boldsymbol{\theta} \qquad (8)$$

$$\mathbf{G}(\boldsymbol{\theta}) = 2\mathbf{B} \qquad (9)$$

Different types of sampling methods may be used to generate the data for the RSM approximation; *Design of Experiments* (DOE), *Latin Hypercube* (LH) sampling and *Monte–Carlo Simulation* (MCS) are some well-known methods. DOE is often used for practical problem in which the true function values are obtained from physical experiments. However this method may also be used for numerical simulation. A hybrid sampling method consists of DOE and LHS may be used for higher order model. *Central Composite Design* (CCD) [10], the most popular class of second-order designs, is used in this paper. It should be noted that although the design often includes a set of centre points, only one centre point should be used in numerical simulation. It also involves the use of a two-level factorial design (or fractional factorial design) combined with $2m$ axial points. Therefore CCD design generates $2^m + 2m + 1$ samples and consequently $2^m + 2m + 1$ flutter deterministic analyses are needed.

It can be readily seen that as the number of parameters m in a 2^m factorial design increases, the number of numerical runs rapidly increases. This increases the computational time considerably especially for industrial sized problems. Fractional factorial design may be used in this case to reduce the number of samples. Any fractional factorial design of resolution m includes complete factorial designs in any subset of $m - 1$ parameters. This concept can be used to reduce the number of runs from 2^m to 2^{m-1}. This is called half-fraction design which is used in this paper. Suppose a system with seven parameters in which full factorial designs requires 128 analyses. The number of samples can be reduced to 64 using half-fraction design. More details about the fraction analysis can be found in [10].

Model adequacy checking is a crucial step in RSA. The residuals from the least-square fit can be used to judge the model adequacy. If the residuals show that the fitted model cannot represent the true function values, then a higher order model or different type of functions may be needed. Another option might be to divide the space of uncertain parameters into regions and consider a quadratic model for each region. It should be noted that the higher order model includes a greater number of regression coefficients and therefore leads to increased computational time.
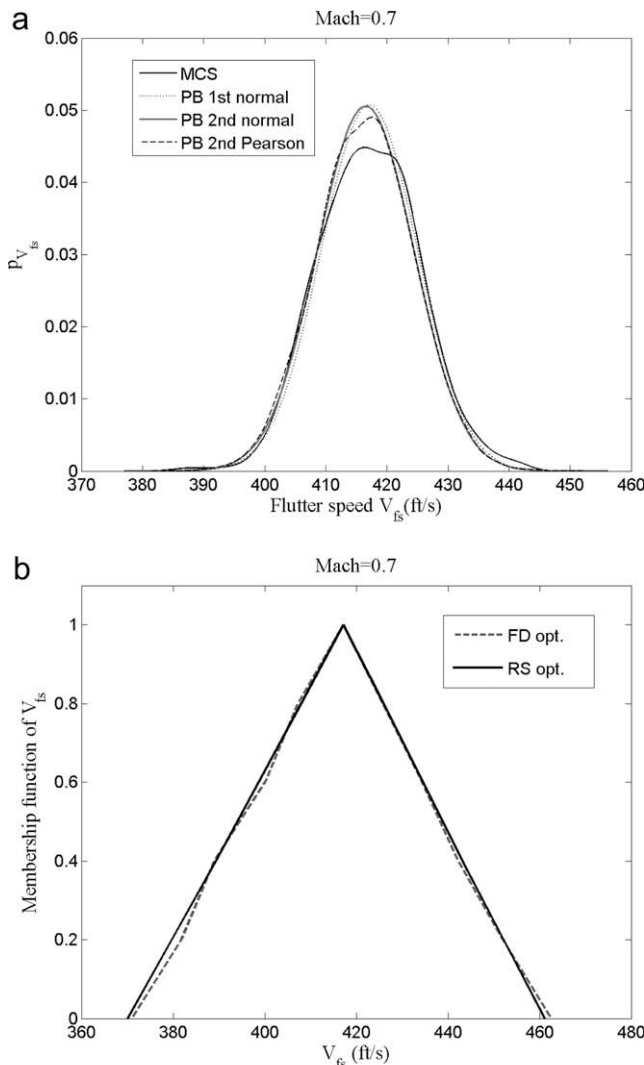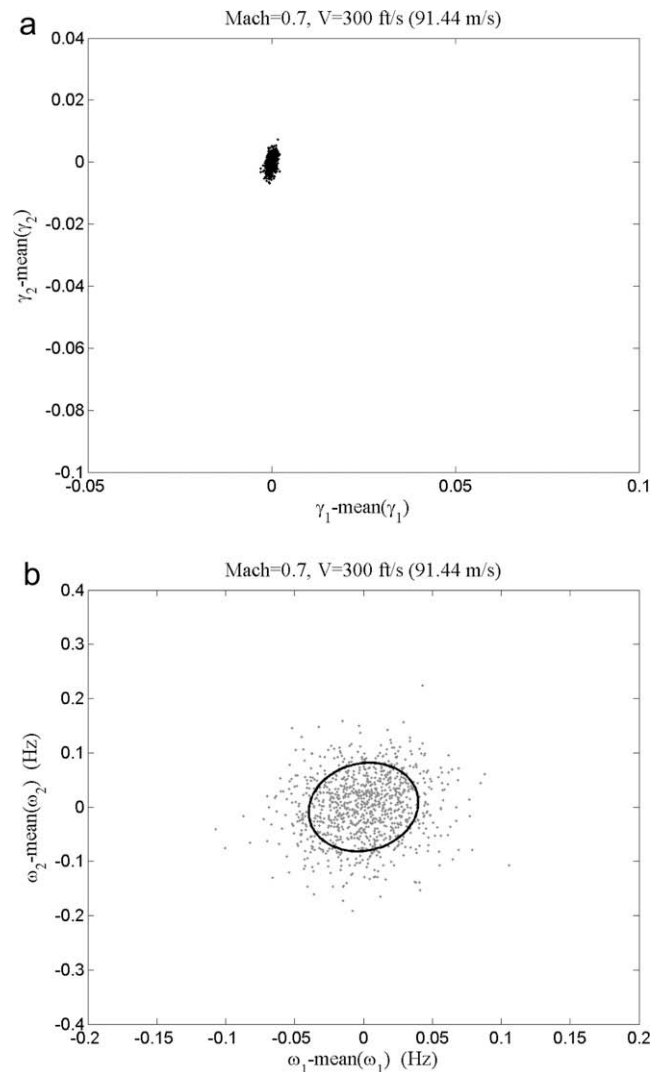

Fig. 10. Flutter speed: (a) pdfs obtained by 1st and 2nd order perturbation and MCS (b) membership function obtained by RSM and FD optimisation.

Fig. 11. Scatter of the aeroelastic eigenvalues at 300 ft/s (91.44 m/s). (a) Damping, and (b) circular frequency.

3. Propagation methods

Uncertainty in numerical models can be represented by intervals, fuzzy sets or probability concepts. Probabilistic models have been the most popular for numerical uncertainty modelling so far. However due to lack of knowledge about the probability distribution of the parameters in the model, there is a growing awareness of intervals and fuzzy methods as will be described in what follows. Sections 3.1 and 3.2 describe the interval flutter analysis and the application of fuzzy logic methods to flutter problems. The probabilistic method, based on perturbation theory, and Monte–Carlo simulation are described in Sections 3.3 and 3.4.

3.1. Interval flutter analysis

The parameter vertex solution [16] is the simplest and most efficient method for interval analysis, but its application is only valid for a restricted class of eigenvalue problems. In particular the eigenvalue problem must be symmetric and linear. As stated before, the eigenvalue problem in Eq. (2) is nonlinear. In addition the matrix **A** is asymmetric. Therefore it is necessary to apply global optimisation procedures in search of the maximum and minimum damping, circular frequency or flutter speed. The optimisation problem may be expressed by the following statement.

Determine,

$$[\underline{y}, \bar{y}] = [\min(y), \max(y)] \tag{10}$$

subject to,

$$[\mathbf{A}(\boldsymbol{\theta}, \omega_i) - \lambda_i \mathbf{I}](\mathbf{u}_i) = \mathbf{0}; \quad \underline{\boldsymbol{\theta}} \leq \boldsymbol{\theta} \leq \bar{\boldsymbol{\theta}} \tag{11}$$

where $\underline{\bullet}$ and $\bar{\bullet}$ represent the lower and upper bounds of $\bullet$ respectively, y is an aeroelastic response such as damping, circular frequency or flutter speed and $\boldsymbol{\theta} \in \mathfrak{R}^{m \times 1}$ is the vector of uncertain system parameters. Different optimisation methods may be used in Eq. (10). The method of *Feasible Directions* (FD) based on Newton's approach [17] is used for global optimisation in this paper. However it is important to choose an efficient optimisation method. The response surface method can also be used for reducing the computational time of optimisation. As mentioned earlier, a quadratic function is used to approximate the aeroelastic response in this paper. Therefore a quadratic optimisation method may be used to evaluate the upper bound and lower bound of aeroelastic responses in Eq. (10). The reflective Newton method [18] for minimisation/maximization of a quadratic function subject to bounds on
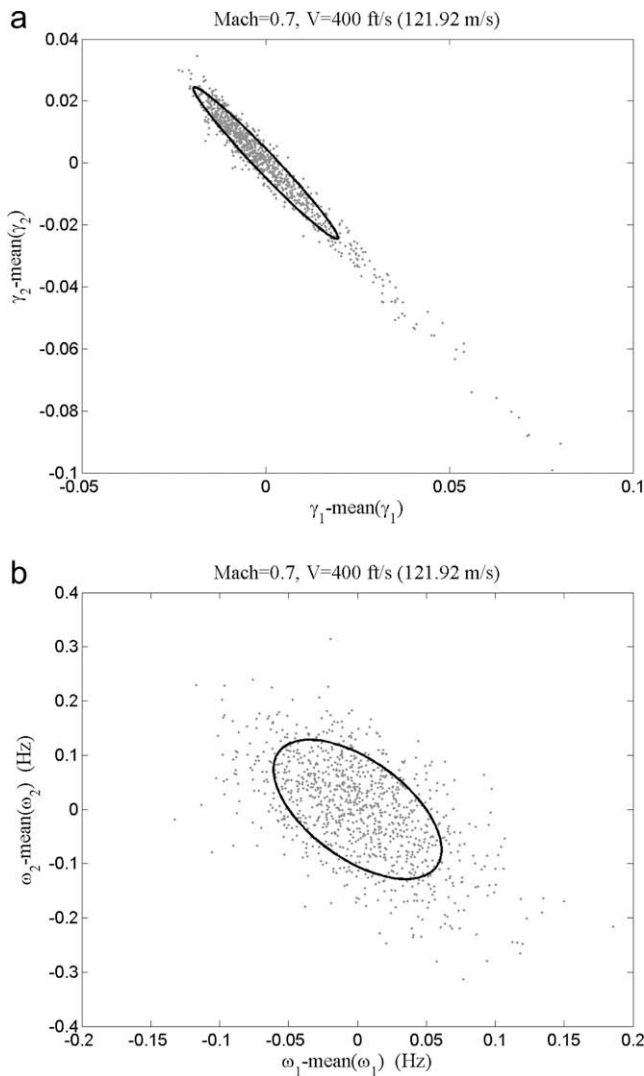
Fig. 12. Scatter of the aeroelastic eigenvalues at 400 ft/s (121.92 m/s). (a) Damping, and (b) circular frequency.
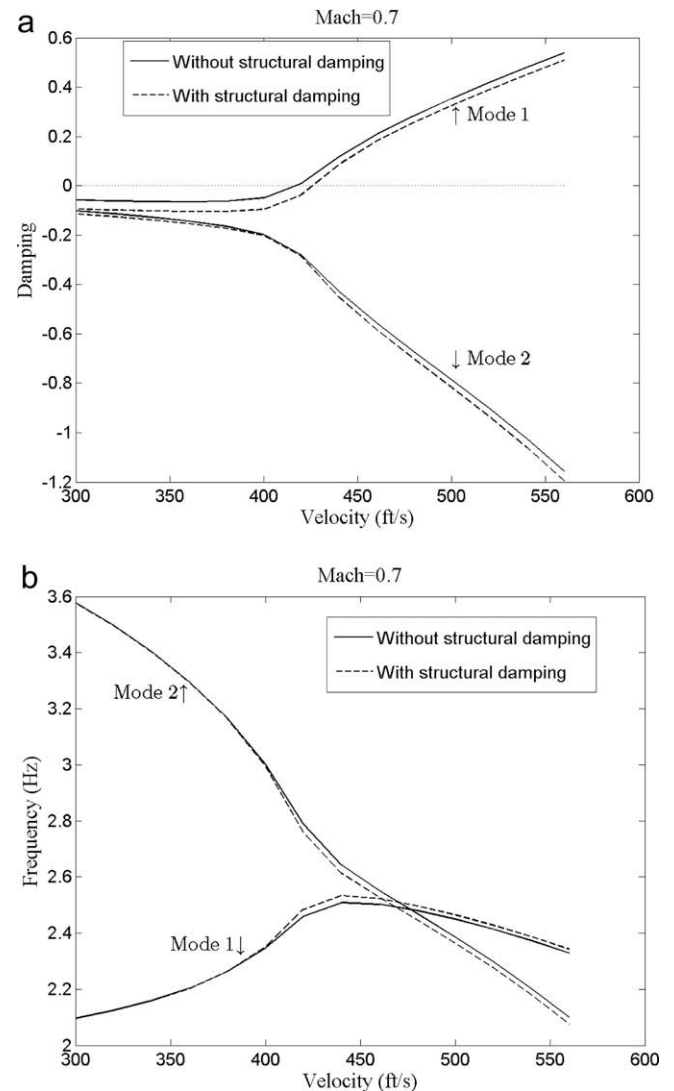
Fig. 13. (a) Damping ratios, and (b) frequencies for modes 1 and 2 with and without damping.
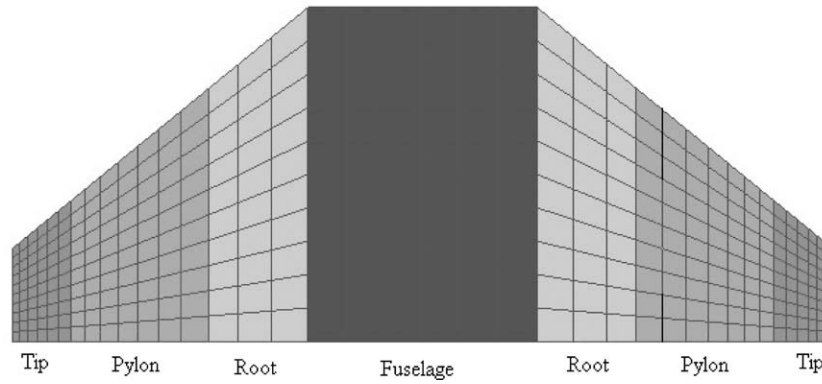
Fig. 14. Parameterisation of the wing.

Table 3
Updated wing-model properties.

	Root	Pylon	Tip
E (GPa)	157.3	96.7	95.6
G (GPa)	62.92	38.68	38.24
ρ (kg/m3)	5680	3780	3780
v	0.25	0.25	0.25
t (m)	0.075	0.03	0.03

variables is used here. The method is available in the optimisation toolbox of MATLAB 2008. Fig. 1 shows a typical graph which shows the interval results for eigenvalue real part of unstable mode and flutter speed. The procedure for interval flutter analysis may be described according to the following steps,

(1) Select uncertain structural parameters from sensitivity analysis and define their intervals.
(2) Generate samples from the space of structural parameters using DOE.
(3) Evaluate the aeroelastic responses at these samples.
(4) Fit a second-order model using the least-square technique.
(5) Find the upper and lower aeroelastic responses using quadratic programming optimisation.

3.2. Fuzzy method

The fuzzy finite element method involves the application of a numerical procedure at a number of α-levels as illustrated in Fig. 2 (reproduced from Moens and Vandepitte [9]). In our particular application the fuzzy-output membership function is the aeroelastic responses such as flutter speed. Fig. 2 shows specifically the procedure for a function of two triangular fuzzy variables with four α-levels. The method is described in detail in [9]. The response surface method can be used for construction of fuzzy membership functions of the output data. In the numerical example in this paper, it is observed that an adequate RSM approximation can be obtained by using a CCD at the mid-level of the fuzzy diagram of

Table 4
Symmetric mode frequencies (Hz).

	Mode 1	Mode 2	Mode 3	Mode 4	Mode 5
Updated FE model	3.74 (h_1)	5.91 ($\alpha+\theta$)	8.12 (γ)	11.00 ($h_2+\alpha$)	11.51 ($\theta_{\alpha T}$)
GVT [29–31]	4.07 (h_1)	5.35 ($\alpha+\theta$)	8.12 (γ)	12.25 (h_2)	

*h_i: ith bending, α: pitch, θ: torsion, γ: yaw, $\theta_{\alpha T}$: tip torsion + pitch.

input parameters. If the samples from axial points of this design are chosen to coincide with the bounds of the lowest α-level of the fuzzy diagram of input parameters then only one response surface at the mid-level is estimated and this model will be used for interval analysis at all the α-levels considered. The computational time for propagation using fuzzy methods is then reduced considerably. Application of RSM for calculating the fuzzy envelope FRFs of models with uncertain properties was investigated by Munck et al. [19].

3.3. Perturbation procedure using the theory of quadratic forms

The uncertain flutter equation may be written as,

$$\left[\mathbf{M}(\theta)\lambda^2(\theta)+\left(-\frac{1}{4}\rho\bar{c}V\mathbf{B}/k(\theta)+\mathbf{C}\right)\lambda(\theta)+\left(-\frac{1}{2}\rho V^2\mathbf{E}+\mathbf{K}(\theta)\right)\right](\mathbf{u}(\theta))=\mathbf{0}$$
(12)

where $\theta\in\Re^{m\times1}$ is the vector of uncertain structural parameter. The aeroelastic response can be expanded about the mean value of the uncertain parameters as,

$$y_i=y_i(\hat{\theta})+\sum_{j=1}^m\frac{\partial y_i}{\partial\theta_j}\bigg|_{\theta_j=\hat{\theta}_j}(\theta_i-\hat{\theta}_i)+\sum_{j=1}^m\sum_{k=1}^m\frac{\partial^2 y}{\partial\theta_j\partial\theta_k}\bigg|_{\substack{\theta_j=\hat{\theta}_j\\\theta_k=\hat{\theta}_k}}(\theta_j-\hat{\theta}_j)$$
$$\times(\theta_k-\hat{\theta}_k)+\dots$$
(13)

where y denotes the aeroelastic response and the partial derivatives are evaluated at the mean values of the structural parameters using Eqs. (8) and (9). According to quadratic theory [11,12] the cumulants of y may be expressed as,

$$m_i^1=y(\hat{\theta})+\frac{1}{2}\text{trace}(G_y(\hat{\theta})\text{cov}(\hat{\theta},\hat{\theta}))$$
(14)

$$m_i^r=\frac{r!}{2}\mathbf{g}_y(\hat{\theta})^T[\text{cov}(\hat{\theta},\hat{\theta})\mathbf{G}_y(\hat{\theta})]^{r-2}\text{cov}(\hat{\theta},\hat{\theta})\mathbf{g}_y(\hat{\theta})$$
$$+\frac{(r-1)!}{2}\text{trace}([\mathbf{G}_y(\hat{\theta})\text{cov}(\hat{\theta},\hat{\theta})]^r),\quad r\geqslant2$$
(15)

where $\mathbf{g}(\theta)$ and $\mathbf{G}(\theta)$ are the gradient vector and Hessian matrix respectively evaluated by RSM at the mean values of structural parameters $\hat{\theta}$. If only the first-order terms are retained then $m_i^{(1)}=\hat{y}=y(\hat{\theta})$, $m_i^{(2)}=\text{var}(y)=\mathbf{g}_y(\hat{\theta})^T\text{cov}(\hat{\theta},\hat{\theta})\mathbf{g}_y(\hat{\theta})$ and $m_i^{(r)}=0$ $r\geqslant3$. Therefore the pdfs of damping and of the flutter speed, may be assumed to be normal distributions,

$$p(y)=\frac{1}{\sqrt{2\pi m_i^{(2)}}}\exp\left(-\frac{(y-m_i^{(1)})}{2\pi m_i^{(2)}}\right)$$
(16)

The pdf of the circular frequency, which is strictly positive, may be assumed to be a truncated Gaussian distribution,

$$p(y) = \frac{1}{\Phi(m_i^{(1)}/\sqrt{m_i^{(2)}})\sqrt{2\pi m_i^{(2)}}} \exp\left(-\frac{(y - m_i^{(1)})}{2\pi m_i^{(2)}}\right) \qquad (17)$$

where Φ is the cumulative Gaussian distribution function. If the Hessian matrix is retained then the first four moments of the aeroelastic responses can be determined using Eqs. (14) and (15). It should be noted that the third and fourth moments are more inaccurate than the first and second moments because of the second-order perturbation used to represent the aeroelastic response. In this case if only the first two moments are considered Eqs. (16) and (17) may be used to estimate the pdf of the aeroelastic response. However if the second-order model is a quite accurate description of the aeroelastic response in the region of structural parameter variation, then the accuracy of higher order moments will be increased. In this case the probability density function may be evaluated using Pearson's theory [20,21]. The pdf is then expressed as a function of the mean and three central moments from 2nd order to 4th order [20,21] as,

$$\frac{dp(y)}{dy} = \frac{a + y}{b_0 + b_1 y + b_2 y^2} p(y) \Rightarrow p(y) = \exp\left(\int \frac{a + y}{b_0 + b_1 y + b_2 y^2} dy\right) \qquad (18)$$

The four coefficients, a, b_0, b_1 and b_2 may be determined as explained in the Appendix B. Finally a large number of samples according to the pdf in Eq. (18) may be generated and the probability density function constructed using Kernel density estimation [22].

3.4. Monte–Carlo simulation

In MCS a large number of samples of the uncertain parameters θ selected from an assumed probability distribution is used to evaluate the aeroelastic responses. The mean values and standard deviations of the outputs may be evaluated directly from the scatter of the responses. Kernel density estimation [22] applied to the discrete responses then results in a continuous probability density function by constructing a weighted sum of Gaussian pdfs centred on each sample.

Whichever propagation method (interval, fuzzy or probabilistic) is used, an issue of very practical significance is the initial estima-

tion of the parameter uncertainty to be propagated. In this paper we address only the uncertainty associated with the structural model. One approach to this problem is to apply stochastic model updating, as described for example by the present authors [23]. Sensitivity analysis [24] must be carried out as an initial step in model updating to define those parameters that have a significant influence on the measured output. Then subset selection [25] allows one to choose columns of the sensitivity matrix most represented in the vector of outputs. This tends to regularise the updating equations and reduces the number of updating parameters to an over-determined system. While this procedure does not guarantee that the uncertainty is correctly located it will lead to an updated model that more accurately represents the dynamical behaviour of the system. By using stochastic model updating it would, in principle, be necessary to carry out ground vibration tests on a sufficient sample of nominally identical aircraft. Then the variability of the structural parameters might be inferred from measured variability in dynamic responses (e.g. variability in measured natural frequencies). A database of information obtained from such an exercise might be deemed applicable to a range of aircraft and not just the particular type of aircraft tested, depending upon design similarities and engineering judgement etc. The application of informed engineering judgement is particularly important in model updating.

4. Numerical examples

4.1. The Goland wing without structural damping

The finite element model of the heavy version of the Goland wing is shown in Fig. 3. Full details of the wing geometry and the finite element model are provided in Refs. [4] and [26]. The NASTRAN model is available from the authors upon request. The wing is composed of upper and lower skins, three spars, eleven ribs, three spar caps, eleven rib caps and 33 posts (1D elements) with nominal, but uncertain, thicknesses and areas as defined in Table 1.

Sensitivity analysis was carried out in order to find the random parameters having most affect on the damping of the aeroelastic modes. The sensitivities of damping with respect to the normalised structural parameters were evaluated at four velocities close to the

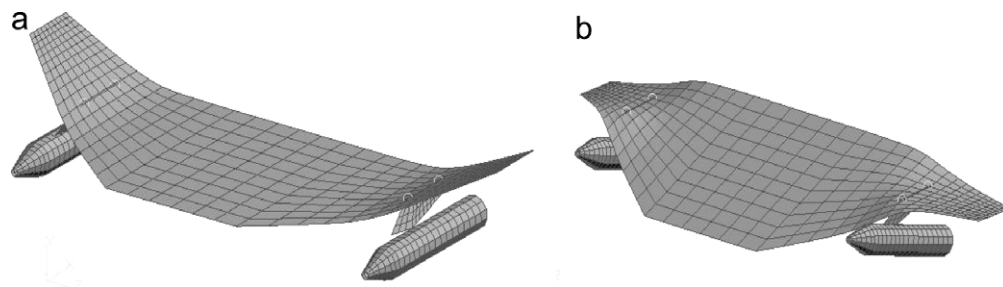**Fig. 15.** Normal modes (a) mode 1, first bending (h_1), symmetric, 3.74 Hz, (b) mode 2, torsion + pitch ($\alpha + \theta$), symmetric, 5.91 Hz.
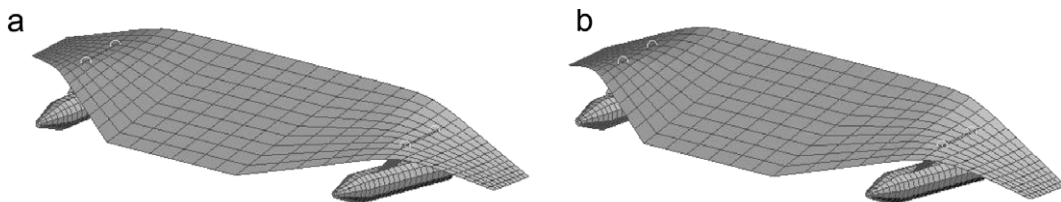

Fig. 16. Aeroelastic modes at velocity 350 m/s, (a) mode 1, 4.106 Hz, (b) mode 2, 4.136 Hz.

flutter speed at different Mach numbers. Solving the deterministic flutter equation at the mean values of the random parameters showed that flutter occurred in the first mode for the complete range of Mach numbers chosen. The sensitivities, scaled to avoid ordering effects, were found to be greater for the lower Mach numbers than the higher ones. Fig. 4 shows the values of the sensitivities for the Mach number of 0.7, where it is seen that among the 63 random parameters, just seven are capable of significantly changing the damping and the flutter speed. The damping ratios were found to be most sensitive to the same seven parameters at different Mach numbers.

For interval analysis, the selected random parameters were considered to be in intervals defined by ±5% of the mean values given in Table 1. The damping and circular frequency of modes 1 and 2 are shown in Fig. 5a and b. MCS was used to verify the results obtained by interval analysis using samples generated from uniform distributions. Fig. 5 shows that a good agreement between results obtained from interval analysis and MCS is achieved. It is also seen in Fig. 5 that the results achieved by RSM optimisation match with those obtained from global optimisation using the method of feasible direction (FD). Also from Fig. 5a it is observed that the flutter speed is defined within the interval from 410 ft/s (125 m/s) to 440 ft/s (134 m/s) at Mach 0.7. Modes 3 and 4 remained stable at all the velocities considered. The flutter-speed bounds versus Mach number are shown in Fig. 6 where it is seen that the interval-analysis and MCS results are in good agreement.

From Fig. 5a and b it can be also seen that whereas the variability of the circular frequency remains unchanged throughout the velocity range, the damping becomes sensitive as the flutter speed is approached and at higher velocities the damping variability becomes similar in extent to the frequency variability. This result demonstrates how the damping becomes dependent upon the mass and stiffness structural parameters at the flutter speed and beyond. At low speeds the damping ratios are mostly unaffected by **M** and **K** variability so that in this range the behaviour is similar to normal-mode structural behaviour. This can be easily shown by calculating the MAC matrix [27] between normal-mode and aeroelastic mode as follows,

$$\mathrm{MAC}(\{\phi_s\}_i, \{\phi_a\}_j) = \frac{|\{\phi_s\}_i^T\{\phi_a^*\}_j|^2}{(\{\phi_a\}_j^T\{\phi_a^*\}_j)(\{\phi_s\}_i^T\{\phi_s^*\}_i)} \quad (19)$$

where $\{\varphi_s\}_i$ is the ith structural normal mode and $\{\varphi_a\}_j$ is the jth aeroelastic mode. $\{\bullet\}^*$ represents the complex conjugate. At low velocities, e.g. 300 ft/s (91.44 m/s), the MAC matrix is,

$$\mathrm{MAC} = \begin{bmatrix} 0.995 & 0.004 \\ 0.062 & 0.931 \end{bmatrix} \quad (20)$$

and at high velocity, e.g. 420 ft/s (128 m/s), the MAC is found to be,

$$\mathrm{MAC} = \begin{bmatrix} 0.897 & 0.013 \\ 0.530 & 0.223 \end{bmatrix} \quad (21)$$

Fig. 7a and b shows the sensitivity of damping ratio and circular frequency of the first two eigenvalues (crossing modes) with respect to thickness of leading edge spar, the most effective parameter from Fig. 4, at different velocities and Mach number 0.7. As it can be seen from Fig. 7a the damping ratios of both modes are insensitive to the uncertain parameter at low velocities and they reach their maximum value at flutter speed regardless of sign. The sensitivity values decrease when the flutter speed is exceeded. Fig. 7b shows that the sensitivities of circular frequencies of both modes reach a maximum at flutter speed. Sensitivity curves of similar symmetric form to Fig. 7a and b were found for the sensitivities of both modes to the other randomised parameters.

Fig. 8 shows the norm of the flutter-speed sensitivity with respect to uncertain parameters versus Mach number. The variability

in structural parameters has more influence on flutter-speed variation at lower Mach numbers.

Gaussian distributions were chosen for the probability perturbation analysis using seven randomised parameters with mean values as in Table 1 and coefficients of variation COV = 0.05 (as in Ref. [4]). Other parameters were taken to be deterministic with values as in Table 1. Propagation methods were applied to the Goland wing to estimate the output pdfs. In MCS, 1000 samples were taken from the parameter pdfs. For propagation by the fuzzy method, the Gaussian probability density functions of system parameters were approximated by triangular membership functions as explained in [28]. The maximum variation of the parameters (i.e. at level α_1) was given by $\delta = \sqrt{2\pi}\sigma$ where σ is a standard deviation of the Gaussian probability density function [28]. First eigenvalue damping distributions by first- and second-order probabilistic perturbation using normal distribution (Eq. (16)) and Pearson's theory (Eq. (18)), and MCS are shown together in Fig. 9a at velocity 400 ft/s (121.9 m/s) and Mach number 0.7. Although the first-order perturbation and second-order perturbation using normal distribution accurately captures most of the pdf generated by MCS, it is clear that there are differences at the tails that might be important from a practical engineering point of view. The tails are better represented by the second-order perturbation using Pearson's theory,
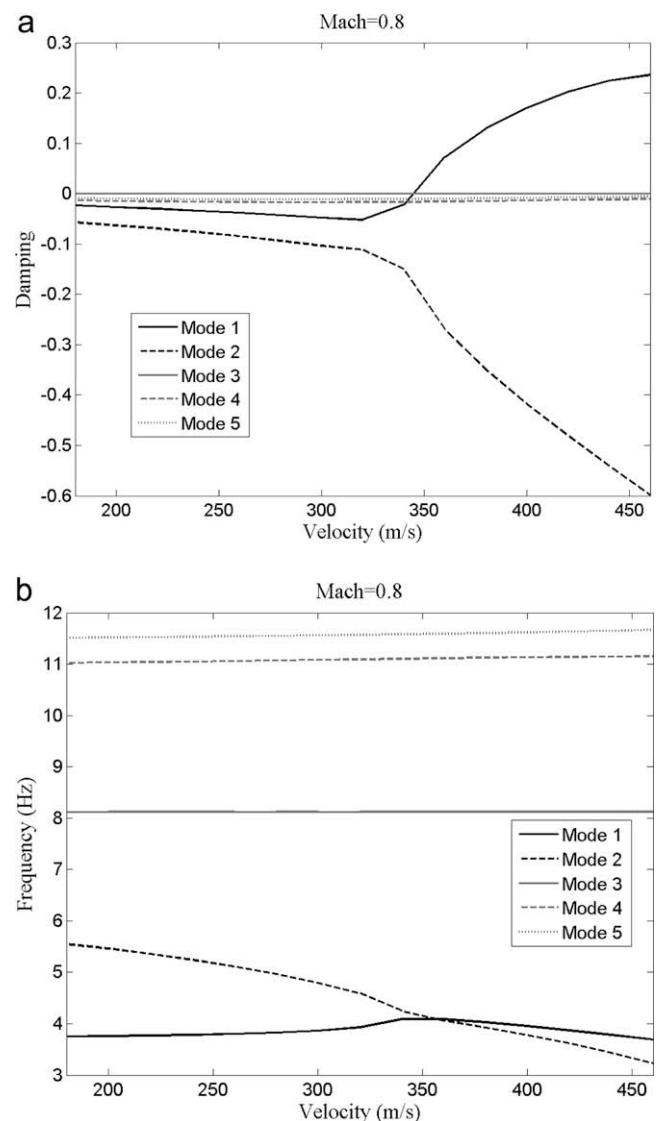

Fig. 17. The damping and frequencies of first five symmetric modes.

which is close to the MCS result at the tails. Fig. 9b shows the fuzzy membership function for the damping (first eigenvalue) at velocity 400 ft/s (121.9 m/s) using FD optimisation and RS optimisation. There is a good agreement between results obtained by the two optimisation methods. Significantly, it is seen from Fig. 9a and b that the fuzzy membership function captures the nonlinearity in the tails of the MCS distributions. In fact the range of variability of aeroelastic-damping variability obtained from the fuzzy method exceeds that determined from MCS. Although, from a strictly mathematical point of view the comparison of statistical distributions with fuzzy membership functions is not allowed, it may still be useful from a practical engineering perspective.

The flutter speed distributions by first- and second-order probabilistic perturbation using normal distribution (Eq. (16)) and Pearson's theory (Eq. (18)), and MCS are shown together in Fig. 10a at Mach 0.7. Two fuzzy membership functions of flutter speed at Mach 0.7 obtained from optimisation method using the method of feasible direction (FD) and RS optimisation are also shown in Fig. 10b. Generally there is a good agreement between the pdfs obtained by perturbation method and pdf generated by MCS. However the second-order perturbation method using Pearson's theory is slightly in better agreement with pdf generated by MCS. From Fig. 10b, it can be seen that the membership function of flutter speed estimated by RS optimisation matches well with membership function of flutter speed achieved by global optimisation using the method of feasible direction (FD).

Table 2 shows the lower and upper bounds of flutter speed obtained from cumulative distribution function of flutter speed from the range of 0.1–99.9% at different Mach numbers. The bounds of zero levels of membership function of flutter speed and the mean values of flutter speed are also shown in Table 2. Generally the bounds achieved by perturbation method are in good agreement with bounds generated by MCS. However, as it can be seen in this table the bounds obtained from second-order perturbation using Pearson's theory are in better agreement with the bounds achieved by MCS at Mach numbers 0.7, 0.8, 0.85 and 0.9. It may be noted, from an engineering point of view, that the bounds of flutter speed

from fuzzy membership functions looks greater than those obtained from probabilistic distributions.

The scatter diagrams in Fig. 11a and b show the variability in the aeroelastic damping and circular frequency at 300 ft/s (91.44 m/s) (below the flutter speed). An ellipse at two standard deviations is superimposed upon the scatter in Fig. 11b. The damping variability is limited to a small condensed area, whereas the aeroelastic frequency variability appears as a random scattering of points over a wider frequency range. Fig. 12a and b shows the scatter of the aeroelastic damping – and aeroelastic frequency at 400 ft/s (121.92 m/s), where it is seen that the scatter diagram for the damping has a particular structure close to a 45° line. We observe that if a scatter point is chosen that corresponds to reduced damping in aeroelastic mode 1 then the damping in mode 2 is increased to a similar degree and vice-versa. We know that the aeroelastic eigenvalues can be expressed as a complex linear combination of the structural normal-mode eigenvalues. Therefore, we can write the first and second complex aeroelastic eigenvalues approximately as,

$$\lambda_1(\boldsymbol{\theta}) \approx \alpha_1 \lambda_1^{(n)}(\boldsymbol{\theta}) + \alpha_2 \lambda_2^{(n)}(\boldsymbol{\theta}) \tag{22}$$

$$\lambda_2(\boldsymbol{\theta}) \approx \beta_1 \lambda_1^{(n)}(\boldsymbol{\theta}) + \beta_2 \lambda_2^{(n)}(\boldsymbol{\theta}) \tag{23}$$

where α_1, α_2, β_1, β_2 are complex functions of velocity and the superscript (n) distinguishes a real structural normal-mode eigenvalue from an aeroelastic eigenvalue. At low velocities α_2, $\beta_1 \rightarrow 0$, α_1, $\beta_2 \rightarrow 1$ (according to MAC matrix given in Eq. (20)) so that the aeroelastic damping values are close to the normal-mode eigenvalues. At higher speeds the complex constants are given more generally by $0 \leqslant |\alpha_1|, |\alpha_2|, |\beta_1|, |\beta_2| \leqslant 1$ (according to MAC matrix given in Eq. (21)) so that the damping values include structural mass- and stiffness-variability present in the normal mode eigenvalues. It appears that at the flutter boundary the uncertainty in the damping has a particular structure that renders the unstable mode less damped while the stable mode is rendered more damped, and vice versa.
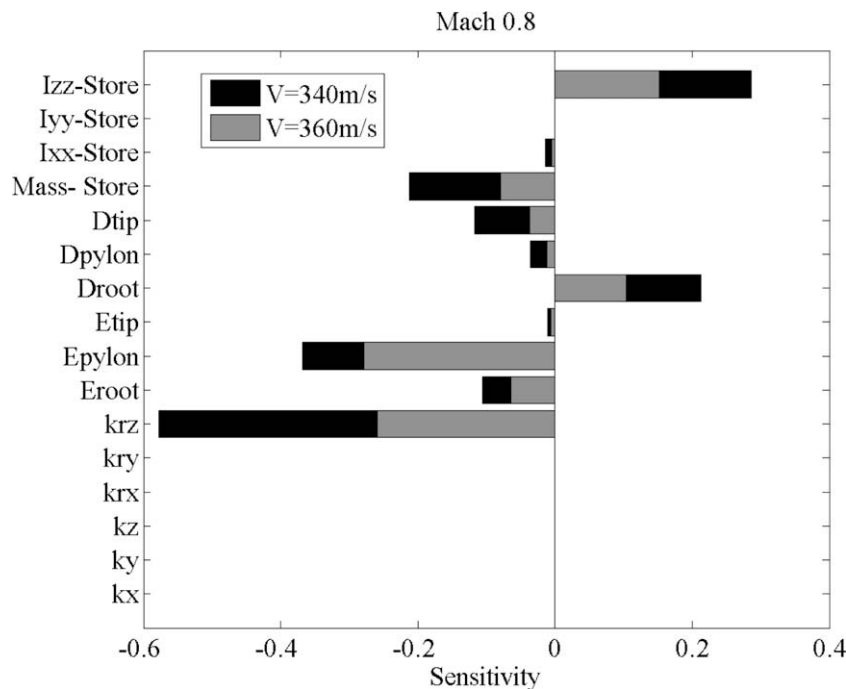

Fig. 18. Sensitivity of the damping (first eigenvalue) to small changes in the scaled parameters (Mach 0.8).

4.2. Goland wing with structural damping

In this section we consider the effect of structural damping on the flutter stability boundaries by adding twelve dashpot elements, uniformly located along the length of the Goland wing from tip to root. Complex eigenvalue analysis was carried out, resulting in modal damping parameters for the first four modes as: 3.403772×10^{-2}, 1.345800×10^{-2}, 4.506277×10^{-2} and 4.539254×10^{-2}, being representative of structural damping in an aircraft wing. The damping and frequency of the aeroelastic eigenvalues for the damped and undamped system are shown at different velocities in Fig. 13a and b, respectively. It can be seen in Fig. 13a that a small but significant increase in the flutter speed is observed when structural damping is included. From Fig. 13b it is seen that the frequencies of the aeroelastic modes are not affected by structural damping at lower velocities but they changed as flutter occurs. Gaussian distributions were chosen for the twelve damping parameters with mean values of 200 lb·s/ft (2919 N·s/m) and coefficients of variation COV = 0.05.

Probabilistic perturbation and MCS was found to result in very narrow bands of variation for the damping, frequency and flutter speed.

The results obtained by different methods from numerous test cases, with and without structural damping, show that reliable flutter boundary estimates may be obtained by a combination of interval analysis and RSM. Therefore it was decided to use interval analysis for the test case described in the following section.

4.3. Generic fighter FE model

The finite element model of a generic fighter wing, based on the model described by Cattarius [29], consists of a fuselage, wings, pylon and stores, all modelled using MSC-NASTRAN QUAD4 elements. The fuselage, pylon and stores were considered to be effectively rigid, having very large values for the elastic modulus assigned to them. The mass properties of the pylon and stores were represented by lumped masses, the masses of the pylon and stores being 161 kg and 1027.5 kg respectively and the principal moments of inertias of the stores, $I_{xx} = 27.5$ kg·m^2, $I_{yy} = I_{zz} = 1000$ kg·m^2. The wing-pylon connection was assumed to be rigid and each store was connected to a pylon by six springs (three translational and three rotational). The wings were divided into three regions, root, pylon and tip as shown in Fig. 14. The Young's modulus and density of each region of the wing was adjusted in order to match the normal mode frequencies with data from a ground vibration test (GVT). Table 3 shows updated wing-model properties. Table 4 shows the first five symmetric natural frequencies from the updated finite element model and the GVT, the latter for the production pylon (PP) [30,31]. Figs. 15 and 16 show the first and second structural normal-mode shapes and aeroelastic mode shapes of the full model. It can be seen from Fig. 16 that both first and second aeroelastic mode shapes at the flutter speed are a combination of the bending mode and store pitch.

An aerodynamic model of the wing was established by dividing the left and right wing into panels with 21 span wise and 11 chord wise grid points and dividing the fuselage with 11 span wise and 11 chord wise grid points. Fig. 17 shows the damping and frequency of the first five symmetric modes. It can be seen that modes 1 (bending) and 2 (torsion + pitch) cross each other at a velocity of 350 m/s.

The sensitivities of the eigenvalues to small changes in the six spring coefficients at the stores attachments, the elastic moduli and mass densities of the three regions of the wing and the mass properties of the stores (total mass and three principal moments of inertia) were determined. Fig. 18 shows the sensitivities of the first eigenvalue to these parameters, only eight of which have a sig-
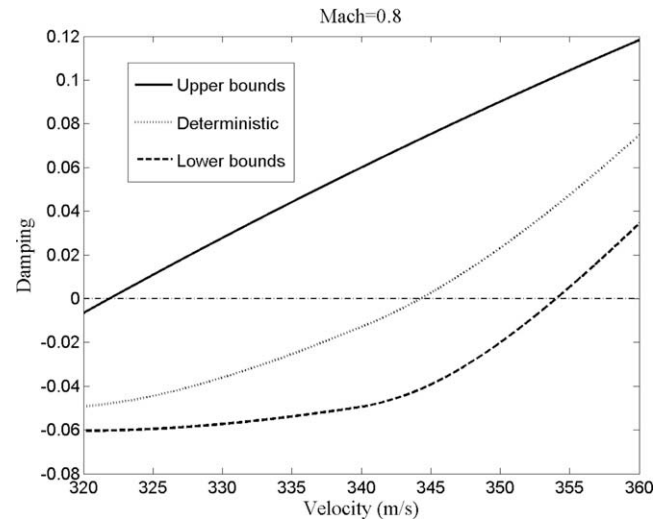

Fig. 19. Bounds on damping for the first eigenvalue determined by interval analysis.

nificant effect on the flutter speed. The pitching spring is the most important parameter. The mass and pitch moment of inertia (z-direction) of the stores were also found to be significant but were not randomised. The reason why the mass and pitch moment of inertia were not included is that they were well defined and therefore should not be randomised. Therefore six uncertain parameters were considered in following intervals:

Rotational spring coefficient: $[0.7–1.3] \times 2000$ kN m/rad.
Young modulus of the root: $[0.9–1.1] \times 1.573 \times 10^{11}$ N/m^2.
Young modulus of the pylon: $[0.9–1.1] \times 9.67 \times 10^{10}$ N/m^2.
Mass density of the root: $[0.9–1.1] \times 5680$ kg/m^3.
Mass density of the pylon: $[0.6–1.1] \times 3780$ kg/m^3.
Mass density of the tip: $[0.9–1.1] \times 3780$ kg/m3.

Fig. 19 shows the interval analysis results for the damping of the first eigenvalue close to the flutter speed. The minimum-bound flutter speed was found to be 322 m/s, considerably lower than the deterministic flutter speed of 343 m/s. The rotational spring coefficient was found to be 1400 kN m/rad, the Young modulus of the root was 1.416×10^{11} Pa, the Young's modulus of the pylon was 8.703×10^{10} Pa, and the mass densities of the root, pylon and tip were 6248 kg/m^3, 2268 kg/m^3 and 3402 kg/m^3, respectively at the minimum flutter speed. Increasing the wing mass at the tip and Pylon and decreasing the mass at root leads to a higher flutter speed, as does a stiffer connection between the store and pylon.

5. Conclusion

Different forward propagation methods, interval, fuzzy and perturbation, were applied to linear aeroelastic analysis for a variety of wing models. Sensitivity analysis was used to select parameters for randomisation that had a significant effect on flutter speed. These random parameters were then propagated through the aeroelastic analysis to obtain estimates of intervals, fuzzy membership functions or pdfs for damping and flutter speed. The response surface method (RSM) is used to approximate the aeroelastic response of the system within the region of variation of uncertain structural parameter. Monte–Carlo simulation (MCS) was used for verification purposes. A combination of response surface method and interval analysis was found not only to be computationally

efficient but also to provide a sufficiently good approximation to flutter bounds determined by MCS. Nonlinear behaviour was observed in tails of the damping pdfs of the flutter mode. Second-order probabilistic perturbation analysis was found to represent the behaviour at the tails with acceptable accuracy. Fuzzy analysis also correctly predicts nonlinear behaviour at the tails. Flutter analysis of the Goland wing showed the instability to be critically dependent upon certain structural mass and stiffness terms. At velocities less than the flutter speed, the intervals of uncertainty on damping were found to be small, but increased at around the flutter speed and beyond to become similar in extent to the bounds on the frequencies across the entire range of frequencies. It was also observed that the variability in structural parameters has more influence on flutter-speed variation at lower Mach numbers. The inclusion of structural damping was found to result in a small but significant increase in the deterministic flutter speed. Structural damping variability had virtually no effect upon the flutter intervals. At velocities close to the flutter speed a particular structure was revealed, close to a 45° line, in the aeroelastic-damping scatter diagrams. Then for a chosen point where the unstable mode was rendered less damped, the stable mode became more damped to a similar degree, and vice-versa. In the analysis of a generic fighter plane flutter instability was found to involve the coupling of wing bending with store pitching behaviour. Flutter bounds were determined by the propagation of structural stiffness parameters (including the pylon – store connection) by interval analysis.

Acknowledgment

Appendix A. List of symbols

M   modal mass
B   modal aerodynamic damping
E   modal aerodynamic stiffness
C   modal structural damping
K   modal structural stiffness
V air speed
ρ air density
k reduced frequency
$\bar{c}$ aerodynamic aerofoil chord
ω_i frequency of mode i
γ_i transient decay rate coefficient, or damping of mode i
$\underline{\bullet}$ the lower bounds of $\bullet$
$\bar{\bullet}$ the upper bounds of $\bullet$
$\hat{\bullet}$ the mean value of $\bullet$
y aeroelastic response
$\boldsymbol{\theta} = [\theta_1 \ \theta_2 \ldots \theta_m]^T$ the vector of uncertain structural parameter
$\mathbf{b} = [\beta_1 \ \beta_2 \ldots \beta_m]^T$ the vector of regression coefficients
g   sensitivity/gradient vector
G   Hessian matrix
ε the vector of residuals
m_i^r rth-order cumulant of the eigenvalues
$\text{cov}(\boldsymbol{\theta}, \boldsymbol{\theta})$ covariance matrix of structural parameters
Φ the cumulative Gaussian distribution function
V_{fs} flutter speed
$|\bullet|$ norm of the vector
∇ gradient operator
p probability density function
$\{\varphi_s\}_i$ the ith structural normal mode
$\{\varphi_a\}_i$ the ith aeroelastic mode
$\{\bullet\}^*$ complex conjugate of complex vector $\{\bullet\}$

Abbreviations
UB   upper bound
LB   lower bound
RS   response surface
FD   feasible direction
Pb 1st   first-order perturbation
Pb 2nd n   second-order perturbation using normal distribution
Pb 2nd p   second-order perturbation using Pearson' theory
FS   flutter Speed
CCD   central composite design

Units
1 ft = 0.3048 m
1 ft^2 = 0.0929 m^2
1 lb = 4.448222 N

Appendix B. Pearson's distribution

According to Pearson's theory [20,21], the probability density function satisfies the differential equation,

$$p'(y) = \frac{a+y}{b_0 + b_1 y + b_2 y^2} p(y) \tag{B1}$$

and the central moments may be calculated as,

$$\mu_i = \int_{-\infty}^{\infty} y p(y) dy \tag{B2}$$

$$\mu_i^{(n)} = \int_{-\infty}^{\infty} (y - \mu_i)^n p(y) dy \quad n = 2, 3, \ldots \tag{B3}$$

From Eq. (B1),

$$[(b_0 + b_1\mu_i + b_2\mu_i^2) + (b_1 + 2b_2\mu_i)(y - \mu_i) + b_2(y - \mu_i)^2]p'(y) \\ = ((a + \mu_i) + (y - \mu_i))p(y) \tag{B4}$$

$$[(b_0 + b_1\mu_i + b_2\mu_i^2)(y - \mu_i)^n + (b_1 + 2b_2\mu_i)(y - \mu_i)^{n+1} \\ + b_2(y - \mu_i)^{n+2}]p'(y) = ((a + \mu_i)(y - \mu_i)^n \\ + (y - \mu_i)^{n+1})p(y) \quad n = 2, 3, \ldots \tag{B5}$$

Knowing that $\lim_{y \to \pm\infty} (y - \mu_i)^n p(y) = 0$ and integrating the left hand sides of Eqs. (B4) and (B5) by parts leads to,

$$-(b_1 + 2b_2\mu_i) = (a + \mu_i) \tag{B6}$$

$$-n(b_0 + b_1\mu_i + b_2\mu_i^2)\mu_i^{(n-1)} - (n+1)(b_1 + 2b_2\mu_i)\mu_i^{(n)} \\ - (n+2)b_2\mu_i^{(n+1)} = (a + \mu_i)\mu_i^{(n)} + \mu_i^{(n+1)} \quad n = 2, 3, 4, \ldots \tag{B7}$$

The central moments, $\mu_i^{(n)}$, in Eqs. (B6) and (B7) can be replaced by cumulants as:

$$\mu_i = m_i^{(1)}, \quad \mu_i^{(2)} = m_i^{(2)}, \quad \mu_i^{(3)} = m_i^{(3)}, \\ \mu_i^{(4)} = m_i^{(4)} + 3(m_i^{(2)})^2 \tag{B8}$$

and the four unknown coefficients, a, b_0, b_1 and b_2, in Eq. (B1) are then determined by Eqs. ((B6)–(B8)) as,

$$\begin{bmatrix} 1 & 0 & 1 & 2m_i^{(1)} \\ 0 & 1 & m_i^{(1)} & (m_i^{(1)})^2 + 3m_i^{(2)} \\ 0 & 0 & 2m_i^{(2)} & 4(m_i^{(1)}m_i^{(2)} + m_i^{(3)}) \\ 0 & 3m_i^{(2)} & 3(m_i^{(1)}m_i^{(2)} + m_i^{(3)}) & 3(m_i^{(1)})^2 m_i^{(2)} + 6m_i^{(1)}m_i^{(3)} + 5m_i^{(4)} + 15(m_i^{(2)})^2 \end{bmatrix} \\ \times \begin{Bmatrix} a \\ b_0 \\ b_1 \\ b_2 \end{Bmatrix} = \begin{Bmatrix} m_i^{(1)} \\ m_i^{(2)} \\ m_i^{(3)} \\ m_i^{(4)} + 3(m_i^{(2)})^2 \end{Bmatrix} \tag{B9}$$

References

[1] Pettit C. Uncertainty quantification in aeroelasticity: recent results and research challenges. J Aircraft 2004;41(5):1217–29.

[2] Melchers RE. Structural reliability analysis and prediction. New York: John Wiley & Sons; 1999.

[3] Poirion F. Impact of random uncertainties on aircraft aeroelastic stability. In: Proceedings of the third international conference on stochastic structural dynamics; 1995.

[4] Kurdi M, Lindsley N, Beran P. Uncertainty quantification of the Goland wing's flutter boundary, AIAA paper 2007-6309, August 20–23; 2007.

[5] Attar PJ, Dowell EH. Stochastic analysis of a nonlinear aeroelastic model using the response surface method. J Aircraft 2006;43(4):1044–52. July–August.

[6] Wang Z, Zhang Z, Lee DH, Chen PC, Liu DD. Flutter analysis with structural uncertainty by using CFD based aerodynamic ROM, AIAA paper 2008-2197, April 7–10; 2008.

[7] Verhoosel CV, Scholcz TP, Hulshoff SJ, Gutiérrez MA. Uncertainty and reliability analysis of fluid–structure stability boundaries. AIAA J 2009;47(1): 91–104.

[8] Chen L, Rao SS. Fuzzy finite-element approach for the vibration analysis of imprecisely-defined systems. Finite Elem Anal Des 1997;27(1):69–83.

[9] Moens D, Vandepitte D. A fuzzy finite element procedure for the calculation of uncertain frequency response functions of damped structures: part 1 – procedure. J Sound Vibr 2005;288(3):431–62.

[10] Myers RH, Montgomery DC. Response surface methodology; process and product optimisation using designed experiments. New York: John Wiley & Sons; 2002.

[11] Mathai AM, Provost SB. Quadratic forms in random variables: theory and applications. New York, NY: Marcel Dekker; 1992.

[12] Adhikari S, Friswell MI. Random matrix eigenvalue problems in structural dynamics. Int J Numer Methods Eng 2007;69(3):562–91.

[13] Albano E, Rodden WP. A doublet-lattice method for calculating lift distributions on oscillating surfaces in subsonic flows. AIAA J 1969;7(2): 279–85.

[14] Nastran MSC. User manual, aeroelastic analysis user's guide; 1994.

[15] Adhikari S. Complex modes in stochastic systems. Adv Vibr Eng 2004;3(1): 1–11.

[16] Qiu Z, Wang X, Friswell MI. Eigenvalue bounds of structures with uncertain but bounded parameters. J Sound Vibr 2005;282(1–2):297–312.

[17] Rao S. Optimisation theory and applications. India: Wiley Eastern Limited; 1979.

[18] Coleman TF, Li Y. A reflective Newton method for minimising a quadratic function subject to bounds on some of the variables. SIAM J Optim 1996;6(4): 1040–58.

[19] Munck MD, Moens D, Desmet W, Vandepitte D. A response surface based optimisation algorithm for the calculation of fuzzy envelope FRFs of models with uncertain properties. Comput Struct 2008;86(10):1080–92.

[20] Suzuki G. A consistent estimator for the mean deviation of the Pearson type distribution. Ann Inst Stat Math 1965;17(1). December.

[21] Pearson K. Contributions to the mathematical theory of evolution, II: skew variation in homogeneous material. Philos Trans R Soc London ARRAY 1895;186:343–414.

[22] Bowman AW, Azzalini A. Applied smoothing techniques for data analysis. Oxford University Press; 1997.

[23] Khodaparast HH, Mottershead JE, Friswell MI. Perturbation methods for the estimation of parameter variability in stochastic model updating. Mech Syst Signal Process 2008;22(8):1751–73.

[24] Mottershead JE, Mares C, Friswell MI, James S. Selection and updating of parameters for an aluminium space-frame model. Mech Syst Signal Process 2000;14(6):923–44.

[25] Friswell MI, Mottershead JE, Ahmadian H. Combining subset selection and parameter constraints in model updating, transactions of the american society of mechanical engineers. J Vibr Acoust 1998;120(4):854–9.

[26] Beran P, Khot N, Eastep F, Snyder R, Zweber J. Numerical analysis of store-induced limit-cycle oscillation. J Aircraft 2004;41(6):1315–26.

[27] Maia NMM, Silva JMM. Theoretical and experimental modal analysis. Research Studies Press, Wiley; 1997.

[28] Hanss M, Willner K. A fuzzy arithmetical approach to the solution of finite element problems with uncertain parameters. Mech Res Commun 2000;27(3): 257–72.

[29] Cattarius J. Numerical wing/store interaction analysis of a parametric F-16 Wing, PhD thesis, Virginia Polytechnic Institute and State University, Blacksburg, Virginia, US; 1999.

[30] Cazier Jr FW, Kehoe MW. Flight test of a decoupler pylon for wing/store flutter suppression. AIAA flight testing conference, AIAA paper 1986–9730; 1986.

[31] Cazier Jr FW, Kehoe MW. Ground vibration test on an F-16 airplane with modified decoupler pylons. Technical memorandum NASA-TM-87634, NASA; 1986.